An Overview of Liquid Spray Modeling Formed by High-Shear Nozzle/Swirler Assembly

Ja Ye Koo*

School of Aerospace and Mechanical Engineering, Hankuk Aviation University, 200-1 Hwajeondong, Duckyangku, Kyunggido, 412-791 Korea

A multi-dimensioanl model is being increasingly used to predict the thermo-flow field in the gas turbine combustor. This article addresses an integrated survey of modeling of the liquid spray formation and fuel distribution in gas turbine with high-shear nozzle/swirler assembly. The processes of concern include breakup of a liquid jet injected through a hole type orifice into air stream, spray-wall interaction and spray-film interaction, breakup of liquid sheet into ligaments and droplets, and secondary droplet breakup. Atomization of liquid through hole nozzle is described using a liquid blobs model and hybrid model of Kelvin-Helmholtz wave and Rayleigh-Taylor wave. The high-speed viscous liquid sheet atomization on the pre-filmer is modeled by a linear stability analysis. Spray-wall interaction model and liquid film model over the wall surface are also considered.

Key Words : Liquid Spray Modeling, Gas Turbine with High-Shear Nozzle/Swirler, reakup of Liquid Sheet, Spray-Wall Interaction

1. Introduction

Gas turbine engines are mainly used for aircraft thrust and power. Gas turbine engines are also used for industrial power generation. Two major challenges to gas turbine engineering are the demands for increased specific fuel consumption and reduced pollutant emissions. Several advances in fuel injection/combustor assembly system are proposed to meet these increasingly demanding next generation gas turbine combustor requirements. Atomization of liquid fuels and subsequent mixing between air and fuel are key issues for obtaining homogeneous fuel-air mixtures in gas turbine combustor. To enhance the mixing of fuel droplets with air in gas turbines, prefilming air blast atomizers with swirl cups assembly are often used for advanced combustion chambers since they deliver a very fine spray almost independently of the fuel flow rate (Mansour et al., 2000; Aigner and Wittig , 1987).

The various atomization processes in gas turbine with high-shear nozzle/swirler assembly are illustrated in Fig. 1. Fuel is discharged from a number of orifices, and liquid jet emanating from the fuel orifices is directed toward the pre-filmer surface, on which a liquid film is formed (Cohen and Rosfjord, 1993). Two radial-inflow inner swirlers and an outer swirler which have counter swirl directions are used to atomize the fuel at the pre-filmer lip. The inner swirler air jet flows along the liquid film and generates waves on its surface. The outer swirler air jet acts on the liquid film at the edge of the pre-filimer surface. The performance of this type of atomizer is affected mostly by the shear stress between the air jets that swirl in opposite directions. Such a counter-current interaction allows reduction of the air flow rate. A dome swirler is additionally used to provide good spray patternation and adequate droplet dispersion. Once vaporization occurs, the

* **E-mail** : jykoo@mail.hangkong.ac.kr
TEL : +82-2-300-0116; **FAX** : +82-2-3158-2191
School of Aerospace and Mechanical Engineering, Hankuk Aviation University, 200-1 Hwajeondong, Duckyangku, Kyunggido, 412-791 Korea. (Manuscript **Received** November 5, 2001; **Revised** December 26, 2002)

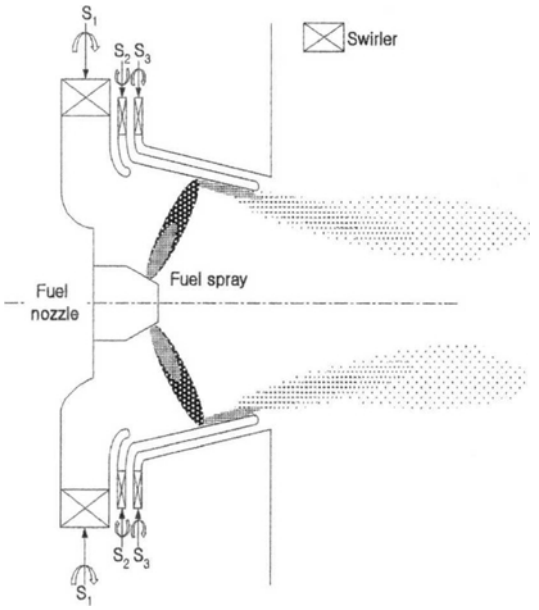

Fig. 1 Schematic of a swirl-stabilized injector in gas turbine

fuel and air mix and burn in the shear layers formed at the edges of the central and outer recirculation zones.

Comprehensive modeling of liquid spray can be found in several references, for example, Reitz (1994), Amsden (1989) and Lin and Reitz (1998), however, each modeling was not integrated for gas turbine spray. This article is devoted to an integrated modeling of spray formation from a liquid jet in a swirl-stabilized injector of the gas turbine engine. The model considers liquid injection through a circular hole, spray impingement on the wall, fuel filming and secondary breakup processes.

2. Breakup Model

Atomization regime is divided into complete spray regime and incomplete spray regime depending on whether or not deformation process of the liquid column vanished (Hiroyasu et al., 1990). As Reynolds number increase in the atomization regime, liquid column may be disintegrated directly due to internal factors which may be originated from turbulences and/or cavitations inside a nozzle. Breakup in the atomization regime is thought to be a result of aerodynamic forces and jet-flow/nozzle conditions.

Aerodynamic theory involves unstable wave growth on the liquid jet surface, on ligaments, or on the windward surface of larger droplets that initially broke off from the main liquid jet. The surface wave perturbation grows with time, driven by the Kelvin-Helmholtz, or the Rayleigh-Taylor instability. The Kelvin-Helmholtz (K-H) instability arises due to a relative shearing motion at a common interface of a two fluids where one fluid flows over another. Ligament and droplet detachments from the surface are brought about by the fastest growing of the unstable surface waves. Droplet sizes are related to the unstable wave length. The Rayleigh Taylor (R-T) instability occurs in the fluid interface when a body force is directed from more dense fluid to the less dense fluid. Any perturbation of this interface tends to grow with time. A liquid sheet (or drop) which is being accelerated by air pressure acting on its surface is subject to possible R-T instability at the sheet (or drop) windward surface.

2.1 Liquid injection

The first stage in the modeling of gas turbine spray formed by high-shear nozzle/swirler assembly is injection of the liquid fuel which is discharged from a number of hole type nozzle orifices. The initial conditions for the calculation of the liquid injection is considered here. Liquid jet breakup is the result of competing, unstable hydrodynamic forces acting on the liquid jet. Hydrodynamic stability theories were applied to study spray atomization using Kelvin-Hemlholtz instability by Reitz (1987). The disintegration of liquid jet was simulated by injecting parcels of liquid in the form of "blobs" that have a characteristic size equal to the nozzle hole diameter, instead of assuming an intact liquid jet at the nozzle exit. The blob size is equal to the nozzle hole diameter, d_0, i.e.,

$$d_{int} = d_0 \tag{1}$$

Figure 2 shows the conceptual liquid flow structure at the nozzle exit for hole type nozzle. The

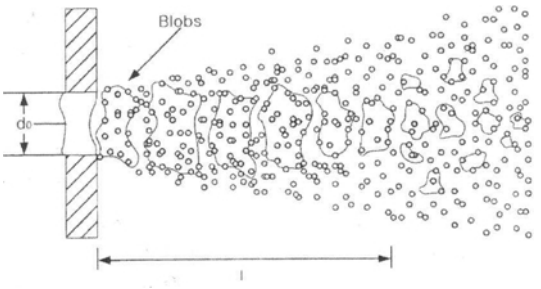

Fig. 2 Conceptual liquid flow structure at the nozzle exit for hole type nozzle (Reitz and Diwakar, 1987)

number of blobs injected per unit time is determined from the mass flow rate. Each blob is assigned with an initial radial velocity component $V_0=U_0\tan(\theta/2)$, where the spray angle, θ, is assumed to be uniformly distributed between 0 and Θ, with

$$\tan\frac{\Theta}{2}=A_1\Lambda_{K-H}\Omega_{K-H}/U_0 \tag{1}$$

U_0 is the injection velocity given by $C_D\sqrt{2\Delta P/\rho_1}$ where ΔP is pressure difference and ρ_1 is density of the liquid. A_1 is a constant equal to 0.188 for a sharp entrance nozzle with a length to diameter ratio of 4-8 (Reitz and Bracco, 1979). Λ_{K-H} and Ω_{K-H} can be determined from linearized hydrodynamic equations.

The maximum growth rate, Ω_{K-H}, which is the frequency of the fastest growing Kelvin-Helmholtz wave, and the corresponding wave length, Λ_{K-H}, are determined as follows.

$$\Lambda_{K-H}=9.02\frac{(1+0.45Z^{0.5})(1+0.4T^{0.7})}{(1+0.87\ We_2^{1.67})}a \tag{3}$$

$$\Omega_{K-H}=\frac{(0.34+0.38We_2^{1.5})}{(1+Z)(1+1.4T^{0.6})}\left(\frac{\sigma}{\rho_1 a^3}\right)^{0.5} \tag{4}$$

where $Z=We_1^{0.5}/R_{e1}$ is the Ohnesorge number, $We_2=\rho_2U^2a/\sigma$, the gas Weber number which is the ratio of the disruptive hydrodynamic force to the surface tension force define, and $T=ZWe_2^{0.5}$ is the Taylor number. σ is surface tension of liquid, a is the blob radius and U is relative velocity between liquid and gas. The subscripts 1 and 2 denote the liquid and gas phases, respectively.

Without blob injection method, the initial drop sizes are assumed to have a size distribution with a SMD given by the correlation.

$$\text{SMD}=\frac{A_2\sigma}{\rho_2U_0^2}$$

where A_2 is arbitrary constant of order of unity.

2.2 Liquid (Blob) breakup using K-H wave model

The next step is a breakup process of the injected liquid column from the hole type nozzle in the high-shear nozzle/swirler assembly. The breakup of liquid droplet moving in a gaseous environment is assumed to be caused by aerodynamic liquid-gas interactions (i.e., shear-flow-induced waves and drag-deceleration-induced waves). The wave model is based Kelvin-Helmholtz type of waves forming on the surface of a cylindrically symmetric liquid blob. The liquid (blob) breakup is modeled by postulating that new drops are formed (with drop radius, r) from a parent drop (with radius, a) with

$$r=C_0\Lambda_{K-H}\quad(C_0\Lambda_{K-H}\leqq a) \tag{5}$$

$$r=\min[(3\pi a^2U/2\Omega_{K-H})^{0.33},\ (3a^2\Lambda_{K-H}/4)^{0.33}]\quad(C_0\Lambda_{K-H}>a,\ \text{one time only}) \tag{6}$$

where C_0 is a constant taken equal to be 0.61 (Reitz, 1987).

Figure 3 shows schematic diagram showing surface waves and breakup on a liquid blob. In Eq. (5), it is assumed that drops are formed with size proportional to the wave length of the fastest growing or most unstable surface wave. In Eq. (6), drops larger than the jet are allowed to produce one time for each injected parcel to prevent product drops from undergoing further unrealistic size increase, and the larger droplet after breakup acts as a new parent drop. The breakup of drops into larger new parent or smaller child drop is determined by tracking the change in the radius of the parent droplet and collecting the mass that would have been shed due to wave stripping and assigning this mass to the child drop. Drop size is determined from the volume of the liquid contained under one surface wave.

As droplets are stripped from the parent parcel, the size of parent parcel is reduced due to the loss

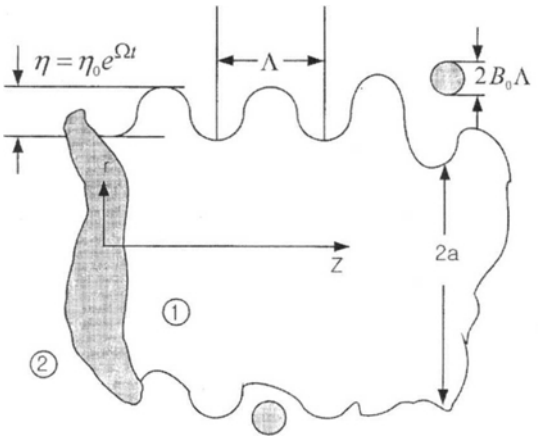

Fig. 3 Schematic diagram showing surface waves and breakup on a liquid blob (Reitz, 1987)

of mass and its characteristic size changes. The rate of change of drop radius in a parent parcel is assumed to obey the following equation.

$$\frac{da}{dt}=-\frac{(a-r)}{\tau_{K-H}} \tag{7}$$

where a is the size of the parent drop, r is the equilibrium droplet size (equal to the child drop size), which is proportional to the most unstable Kelvin-Hemlholtz wavelength found in Eq. (3), $\tau_{K-H}=3.726C_1a/\Lambda_{K-H}\Omega_{K-H}$ with C_1 being an arbitrary breakup time constant, which is suggested to be between 10 and 60.

2.3 Hybrid liquid breakup model using K-H and R-T wave model

Chang et al. (1995) suggested transient breakup model and compared their model with Phase Doppler measurements where hybrid breakup model was suggested using Kelvin-Hemlholtz (K-H) wave model and Rayleigh-Taylor (R-T) wave model. When a liquid sheet which has uniform thickness is accelerated by air pressure acting on its upper surface, the behavior of the upper surface of a sheet of heavier density can be described by R-T instability. The amplitude of the disturbance on the unstable fluid surface for a vertical downward acceleration at any time is given as follows (Taylor, 1963),

$$\eta=\eta_0\cosh\sqrt{2ks\frac{g_1-g}{g_1}\frac{\rho_1-\rho_2}{\rho_1+\rho_2}} \tag{8}$$

where η_0 is initial amplitude of the disturbance, k is wave number ($k=2\pi/\lambda$), g_1 is the liquid sheet or droplet acceleration in the direction of travel and g is the acceleration due to gravity in the direction of travel. The subscript 1 and 2 designate liquid and gas phase. The most rapidly growing frequency is given by

$$\Omega_{R-T}=\left\{\frac{2}{3(3\sigma)^{1/2}}\frac{[(g_1+g)(\rho_1-\rho_2)]^{3/2}}{\rho_1+\rho_2}\right\}^{1/2} \tag{9}$$

The corresponding wave number is given by

$$\Lambda_{R-T}=\frac{[(g_1+g)(\rho_1-\rho_2)]^{1/2}}{(3\sigma)^{1/2}} \tag{10}$$

Upon replacing the acceleration term with the dimensionless Bond number and using the characteristic time constant as $\tau=1/\Omega$, the dimensionless breakup time, T_{R-T}, can be defined and written as follows (Simpkins and Bales, 1972).

$$T_{R-T}=t_{R-T}\frac{U(\rho_1/\rho_2)}{a} \tag{11}$$

$$T_{R-T}=31\mathrm{Bo}^{-\frac{1}{4}} \tag{12}$$

where t_{R-T} is dimensional time, Bo is bond number, which is the ratio of the acceleration induced body force to the surface tension force, giving $\mathrm{Bo}=\rho_1 ga^2/\sigma$ where a is the diameter of drop. The Bond number is expressed in terms of drag coefficient and Weber number using the drag force relation.

$$\mathrm{Bo}=\frac{3}{8}C_D We_2 \tag{13}$$

Beforeis t_{R-T} reached, K-H instability or boundary layer stripping is applied at the edge of the flattened parcel. After t_{R-T} is reached R-T, instability is applied. Once the effects of R-T instability manifest themselves, fragmentation occurs extremely rapidly because the growth rate of the surface waves is exponential.

The radius of the new equilibrium or stable droplet based on R-T instability is given by

$$r=\frac{\pi C_2}{\Lambda_{R-T}} \tag{14}$$

where C_2 is arbitrary constant and which is suggested to be between 0.1 and 0.3 (Xin et at., 1998). Figure 4 shows the comparison of simulated transient droplet velocities with experi-

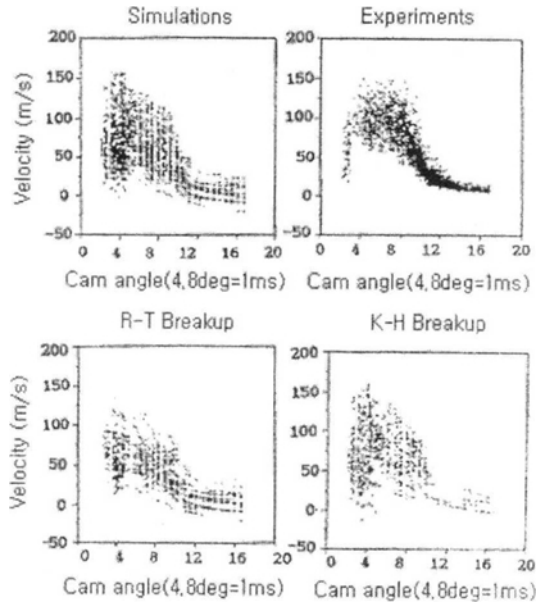

Fig. 4 Comparison of droplet velocities from K-H and R-T hybrid breakup model with experimental data

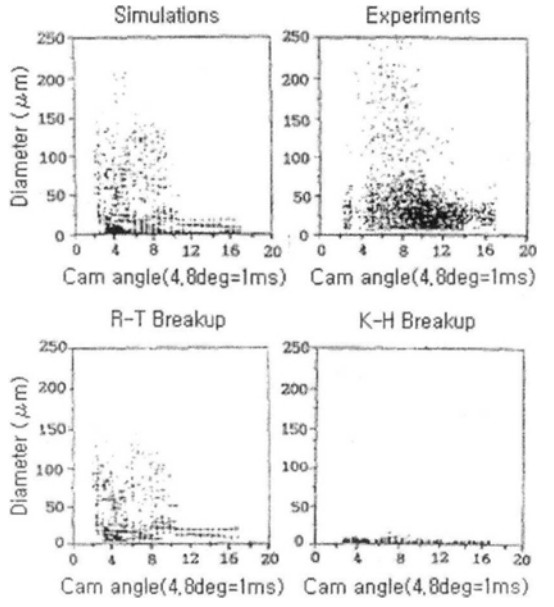

Fig. 5 Comparison of droplet sizes from K-H and R-T hybrid breakup model with experimental data

mental data obtained by PDPA at 30 mm from nozzle tip in the gas pressure of 2.17 MPa. Figure 5 shows the comparison of simulated transient droplet sizes with experimental data obtained by PDPA at 30 mm from nozzle tip in the gas pressure of 2.17 MPa. Droplets produced from R-T instability breakup model ranges small sizes to large sizes. Droplets produced from R-T instability is consisted of droplets from leading edge of the main column and separated large droplets. The parcels which are separated from the main column are subject to the subsequent breakup process. Droplet produced from K-H instability breakup model, which is only applied to the jet column for surface stripping, ranges only to small sizes.

2.4 Drop breakup using wave model

Droplet breakup models can be classified into three categories (Bower et al., 1988); deformation induced breakup (bag breakup), boundary layer stripping (BLS), and surface instabilities (K-H and R-T instabilities). Pilch (1981) modeled the drop breakup depending on Weber number. Droplets break up due to the bag breakup mechanism when

$$25 > We_2 > 6 \tag{15}$$

Remind We_2 is gas Weber number based on gas density, droplet radius, and relative velocity.

Deformation of liquid drop is made by the non-uniform dynamic pressure distribution on the drop surface, and then a thin hollow bag in the center forms and grows while it is attached to a more massive toroidal rim. Bag disintegration and rim disintegration form a large number of small fragments. Droplets break up due to the sheet striping mechanism (Pilch BLS) when

$$175 > We_2 > 50 \tag{16}$$

In sheet striping, no bags are formed; instead, a thin sheet of liquid is swept along the windward surface to the drop equator, where the sheet detaches and is carried into the wake. Beyond the sheet stripping regime, Droplets break up due to the wave crest stripping and catastrophic mechanism when

$$We_2 > 175 \tag{17}$$

In wave crest stripping, short-wave length, large-amplitude waves are formed on the windward

surface of the drop and continuously eroded by the action of the flow field over the surface of the drops. In catastrophic breakup, long-wave length, large-amplitude waves penetrate the drop, and then create several large fragments before large portion of drop mass is reduced by wave crest stripping. Pilch (1981, 1987) insisted that R-T instability plays a dominant role in the acceleration driven environments.

Ranger and Nicholls (1969) suggested another criteria for boundary layer stripping mechanism, where boundary layer is stripped from the periphery of the droplet due to the shearing action of the high speed gas on the droplet surface. For a given flow, droplets break up by a boundary layer stripping mechanism(Ranger-Nicholls BLS; R-N BLS) when

$$We_2/\sqrt{Re_2}>0.5 \tag{18}$$

where the Reynolds number $Re_2=2Ua/\nu_2$, and ν_2 is the kinematic viscosity of the gas. Now consider bag breakup and BLS breakup. The lifetimes of unstable drops are

$$t_{bag}=D_1\sqrt{\rho_1 a^3/\sigma} \tag{19}$$

and

$$t_{BLS}=D_2\frac{a}{U}\sqrt{\rho_1/\rho_2} \tag{20}$$

for the bag and BLS modes, respectively. The constants D_1 and D_2 are of order unity (Nicolls, 1972).

In the wave model, droplets are shed from the parent droplet throughout the parent droplet life time. New parcels of droplets can be added each time step if the condition is satisfied. The stability criteria Eqs. (15) and (18) are checked each drop parcel at each time step. For a lifetime given by Eqs. (19) and (20), if either of the two criteria continued to be met, a new drop size of parcel is specified using either Eq. (15) or Eq. (18). The rate of change of drop radius with time is as follows.

$$\frac{da}{dt}=-\frac{(a-r_{stable})}{\tau}$$

where τ is lifetime of unstable drops. For a bag breakup, $\tau=t_{bag}$ and $r_{stable}=6\sigma/\sigma_2U^2$. For a BLS breakup, $\tau=t_{BLS}$ and $r_{stable}=\sigma^2/2\rho_2U^2\nu_2$.

2.5 Talyor analogy for drop breakup

TAB (Talyor Analogy Breakup) model was proposed by O'Rourke and Amsden (1987), in which droplet behavior is compared to an oscillating spring-mass system. The external force acting on the mass, the restoring force of the spring, and the damping force are analogous to the gas aerodynamic force, the liquid surface tension force, and the liquid viscosity force, respectively. The TAB model has several advantages. Most of the breakup models use a critical Weber number to decide the occurrence of the droplet breakup. But experiments have shown that there is no unique critical Weber number and the occurrence of breakup depends on the history of its velocity relative to the gas. The history effects are included in the TAB model by solving the transient equation for drop oscillation. Moreover, the effect of viscosity is important for small drops and it is included in the TAB model.

Let x be the displacement of the equator of the drop from its equilibrium position. The dimensionless oscillation parameter, $y=2x/r$, is calculated by solving the spring-mass analogy equation,

$$\frac{d^2y}{dt^2}=\frac{2}{3}\frac{\rho_g}{\rho_1}\frac{U^2}{r^2}-\frac{8\sigma}{\rho_1 r^3}y-\frac{5\mu_1}{\rho_1 r^2}\frac{dy}{dt} \tag{21}$$

where U is the relative velocity between the gas and droplet, r is droplet radius, and σ is liquid surface tension.

If U is constant, the solution to the above equation can be obtained as,

$$y(t)=\frac{We}{12}=e^{-t/t_d}\left[\left(y(0)-\frac{We}{12}\right)\cos\omega t+\frac{\dot{y}(0)}{\omega}+\frac{y(0)-\frac{We}{12}}{\omega t_d}\sin\omega t\right] \tag{22}$$

where $We=\rho_1U^2r/a$, which is Weber number, $t_d=\frac{2\rho_1r^2}{5\mu_1}$, which is viscous damping time, ω is oscillation frequency defined by $\omega^2=8\frac{\sigma}{\rho_1r^3}-\frac{1}{t_d^2}$. O'Rouke and Amsden (1987) argued that when the value of y exceeds unity, the droplet breaks up into smaller droplets with the distribution of sizes specified as described below.

In order to check for the occurrence of breakup, the above parameters are evaluated at several stages. Depending on the sign of w^2, breakup occurs or not. If $\omega^2<0$, it occurs in case of over-damped condition for small drops, the oscillation of the droplet is negligible and breakup is unlikely to occur. Then, the parameters y and $\dot{y}\left(=\frac{dy}{dt}\right)$ are set to zero. If $\omega^2>0$, the amplitude of the undamped oscillation is calculated. The amplitude is given by the following expression.

$$A^2=\left(y-\frac{We}{12}\right)^2+\left(\frac{\dot{y}}{\omega}\right)^2 \tag{23}$$

If $(We/12+A)<1.0$, the value of y will never exceeds 1.0 and thus breakup will not occur. The value of y and y are updated using the following expressions. Most droplets will pass the test $(We/12+A)<1.0$.

$$y^{n+1}=\frac{We}{12}+e^{(-\Delta t/t_d)}\left[\left(y^n+\frac{We}{12}\right)\cos\omega\Delta t+\frac{1}{\omega}\left(\dot{y}_n+\frac{y^n-\frac{We}{12}}{t_d}\right)\sin\omega\Delta t\right] \tag{24}$$

$$\dot{y}_{n+1}=\frac{\left(\frac{We}{12}-y^{n+1}\right)}{t_d}+e^{(-\Delta t/t_d)}\left[\left(\dot{y}_n+\frac{y^n-\frac{We}{12}}{t_d}\right)\cos\omega\Delta t-\omega\left(y^n-\frac{We}{12}\right)\sin\omega\Delta t\right] \tag{25}$$

If $(We/12+A)>1.0$, breakup is possible in the current time. In this case, the breakup time is calculated as the smallest root of the following equation

$$\frac{We}{12}+A\cos[\omega(t-t^n)+\phi]=1 \tag{26}$$

where
$$\cos\phi=\frac{y^n-We/12}{A} \tag{27}$$

and
$$\sin\phi=-\frac{\dot{y}^n}{Aw} \tag{28}$$

If the breakup time is greater than time t_{n+1}, no breakup occurs in the current time step and hence the y and $\dot{y}$ values in Eq. (24) and (25) are updated. If the breakup time is greater than t_n and less than t_{n+1}, then breakup occurs in the current time step and $\dot{y}$ is evaluated at breakup time. The radius of product droplets can be determined from the energy balance between parent droplets and product droplets. The radius of product droplet is chosen randomly from χ-square distribution. The Sauter mean diameter (r_{32}) of the product droplet is calculated by the following expression

$$r_{32}=\frac{r}{\frac{7}{3}+\frac{1}{8}\frac{\rho_1 r^2}{\sigma}\dot{y}^2} \tag{29}$$

The direction of the product drop is randomly chosen in a plane normal to the relative velocity vector. Following breakup, the displacement and distortion of the product drop is set to zero.

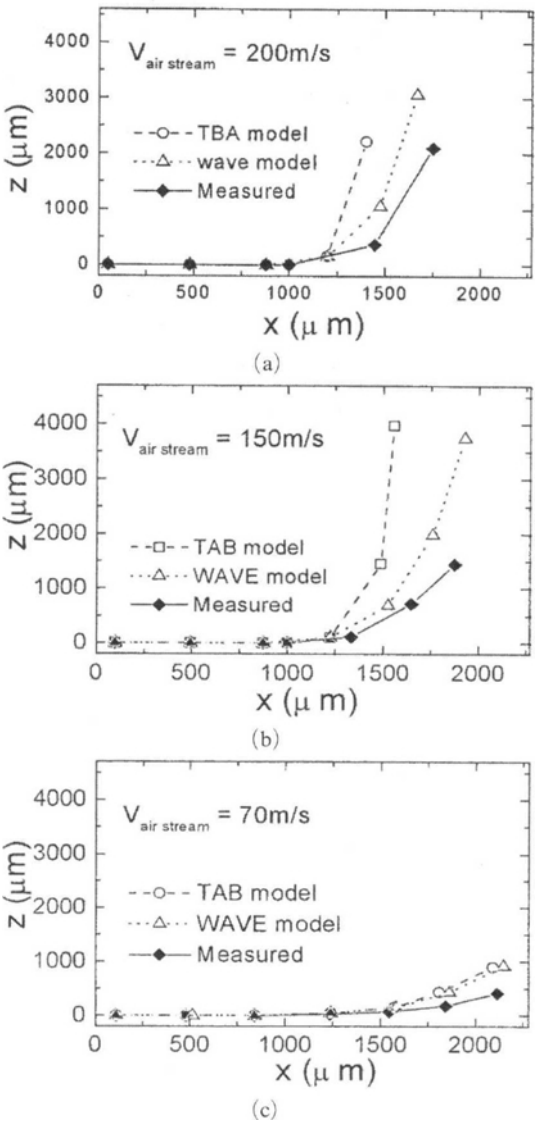

Fig. 6 Comparison of wave model and TAB model for the fuel droplets in high speed air stream

Hwang and Koo (1997) compared droplet behavior which is injected in the high speed cross flow using the wave break model and TAB break model. As shown in Fig. 6, wave break model represents experimental drop behavior better than TAB break model because TAB break model overestimate the droplet drag coefficient. But at low air stream velocity two model showed almost same trajectory.

3. Impingement Model

Liquid jet emanating from the fuel orifices in Fig. 1 is directed toward the pre-filmer surface and impinged on the wall of the pre-filmer. Some of the impinged spray on the wall are bounded, stick, and form a liquid film. Spray-wall interaction model and liquid film model are surveyed here.

3.1 Drop-wall interaction model

The impact of droplets on walls may produce a wide variety of consequences, depending on the size, velocity and material of the impacting elements and the nature of the surfaces. Droplets may adhere, bounce or shatter. The liquid deposited on the surface may retain its droplet form or merge into a liquid film. For a gas turbine spray, which is formed by a prefilming airblast injector, a collection of drops impinge onto the wetted surface successively. A train of drops with a known frequency exists such that each impinging drops feel the effects of its neighboring drops. The collision of a drop with a liquid surface, where the wall temperature (T_w) is less than the liquid boiling temperature (T_B), may result in sticking, bouncing, spreading, or splashing depending on incident drop Weber number. The followings are based on the paper of Stanton and Rutland (1996, 1998)

3.1.1 Stick regime

The stick regime occurs when an impinging drop adheres to the film surface in nearly a spherical form. The transition criteria for the stick regime is $We_d<5$, where the We_d is calculated using the normal velocity of the incident drop.

$$We_d=\frac{\rho d_d V_{d,n}^2}{\sigma} \tag{30}$$

where d_d is a diameter of impinging drop. A drop that is in this regime is assumed to coalesce completely with the liquid film.

3.1.2 Rebounding regime

The rebound regime occurs when the impinging drop bounces off the film when the impact energy is low. The transition criteria for the rebounding regime is $5<We_d<10$. In this regime, the rebound drop velocity magnitude and direction need to be determined. The normal and tangential components of the droplet post-impingement rebound velocity relative to the wall are given by

$$\vec{V}_{d,n}^{p}=-e_n\vec{V}_{d,n} \tag{31}$$

$$\vec{V}_{d,t}^{p}=e_t\vec{V}_{d,tn} \tag{32}$$

where $\vec{V}_{d,n}^{p}$ is the rebounding drop normal velocity; $\vec{V}_{d,t}^{p}$ is the rebounding drop tangential velocity; $\vec{V}_{d,n}^{p}$ is the incident drop normal velocity; and $\vec{V}_{d,t}^{p}$ is the incident drop tangential velocity.

The normal and tangential restitution coefficients, e_n and e_t, are determined from the following equation (Matsumoto et al., 1970).

$$e_n=0.993-1.76\Theta+1.56\Theta^2-0.4\rho\Theta^3 \tag{33}$$

where Θ is the incidence angle of impingement measured from the wall surface.

$$e_t=5/7 \tag{34}$$

3.1.3 Spreading regime

The spreading regime is similar to the stick regime but occurs at higher We_d. The droplet spreads out along the wall surface creating a wall film (in the case of a dry wall) or merging with an existing film on a wetted wall. The transition criteria for spreading is

$$10<We<18.0^2 d_d\left(\frac{\rho}{\sigma}\right)^{\frac{1}{2}}\nu^{\frac{1}{4}}f^{\frac{3}{4}} \tag{35}$$

where ρ, σ, ν, and f are the drop density, surface tension, kinematic viscosity, and drop frequency, respectively. The drop frequency, f, is known as the splashing threshold for multi-drop impact with a thin liquid film and it is calculated by:

$$f=\frac{\vec{V}_{d,t}}{d_d} \tag{36}$$

The droplet loses its velocity component normal to the wall, and its post-impingement velocity relative to the wall is :

$$\vec{V}_d^p=\vec{V}_{d,t} \tag{37}$$

$$\vec{V}_{d,t}=\vec{V}_d-\vec{V}_{d,n} \tag{38}$$

where $\vec{V}_d$ is the incident droplet velocity.

3.1.4 Splashing regime

The splashing regime occurs at high impact energy. Upon impact, a crater is formed with a crown at the periphery where liquid jets become unstable and breakup into many secondary droplets. The transition criterion for the splashing regime is

$$We_d>18.0^2 d_d\left(\frac{\rho}{\sigma}\right)^{\frac{1}{2}}\nu^{\frac{1}{4}}f^{\frac{3}{4}} \tag{39}$$

Details of the splashing calculations can be found in the appendix of the SAE paper 980132 (Stanton and Rutland, 1988).

3.2 Liquid film model

The liquid film model is based on the physics involved with a fuel film flow over a solid surface. The major physical processes affecting the liquid film are shown in Fig. 7. The continuity and momentum equations are applied to each wall film cell. The liquid film is assumed to be thin enough so that the incompressible boundary layer approximation can be applied and reduced to a two dimensional film flowing across a three-dimensional surface. The mass flux due to incident drops that impinge is averaged over the wall surface cell area. The lost tangential momentum of impinging drops is added to the film tangential momentum. The velocity profile in the cross-film direction is prescribed to be either laminar or turbulent, and the temperature profile is prescribed to be piecewise linear (Stanton and Rutland, 1996 and 1998 ; Bai and Gosman, 1966 ; Foucart et al., 1988).

After integrating in the cross-film, the continuity equation becomes

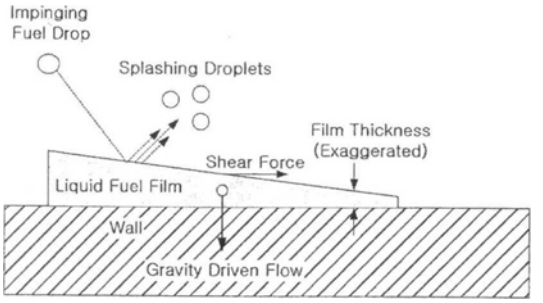

Fig. 7 The physical processes on the liquid film flow (Stanton, 1996)

$$\frac{\partial h}{\partial t}+\frac{1}{A_{wall}}\sum_{i=1}^{N_{side}}(\vec{V}_f\cdot\hat{n})_i h_i l_i =\frac{S_d}{\rho_l A_{wall}}+\frac{\dot{M}_{vap}}{\rho_l A_{wall}} \tag{40}$$

where A_{wall} is the wall cell area, $\vec{V}_f$ is the film velocity, l_i is the length of side i, ρ_l is the film density, h_i is the film thickness at side i. S_d is a source term, which is the mass flux of drops that impinge upon the film or secondary droplets that leave the film which result from splashing, and $\dot{M}_{vap}$ is the rate of fuel vaporization.

The momentum equation is transformed into the following form :

$$\frac{\partial(h\vec{V}_f)}{\partial t}+\frac{1}{A_{wall}}\sum_{i=1}^{N_{side}}\vec{V}_f(\vec{V}_f\cdot\hat{n})_i h_i l_i\phi_i =-\frac{\sum_{i=1}^{N_{side}}(P\hat{n})h_i l_i}{\rho_l A_{wall}}+\vec{g}h+\frac{M_{tang}}{\rho_l A_{wall}}+\frac{\sum_{i=1}^{N_{side}}(\vec{\tau}A_i)}{\rho_l A_{wall}}+\vec{a}h \tag{41}$$

where

$$\phi=\frac{1}{1-\frac{\delta_t}{h}}-\frac{\Theta_t}{h}\frac{1}{\left(1-\frac{\delta_t}{h}\right)^2} \tag{24}$$

The displacement thickness, δ_t, and the momentum thickness, Θ_t. in Eq. (42) can be calculated once the velocity profile in the cross-film direction has been chosen.

The pressure term, P, includes the dynamic pressure, p_d, which results from the incident drop impingement and splashing effects, and the free-stream pressure (gas pressure), p_{wall}.

$$P=p_{wall}+p_d \tag{43}$$

$$p_d=\rho_l \sum_{k=1}^{N_{drop}} \vec{V}_{d,n}^2 \frac{A_{dk}}{A_{wall}}+\rho_l \sum_{j=1}^{N_{splash}} \vec{V}_{d,nj}^2 \frac{A_j}{A_{wall}} \quad (44)$$

where $\vec{V}_{d,n}$ is the normal component of velocity incident drop and $\vec{V}_{d,nj}$ is normal component of velocity of the j-th secondary droplet resulting from splashing.

The tangential momentum contributes to the film as a result of spray impingement and splashing of secondary droplets.

$$M_{\text{tang}}=\sum_{i=1}^{N_{drop}} (m_i \vec{V}_{d,nj}) - \sum_{j=1}^{N_{splash}} (m_j \vec{V}_{tj}) \quad (45)$$

The viscous film term is calculated as follows

$$\sum_{i=1}^{N_{edge}} (\vec{\tau}_i A_i)=\sum_{j=1}^{N_{side}} (\vec{\tau}_{edge\,i} h_j l_j)+\vec{\tau}_{wall} A_{wall}+\vec{\tau}_{liq/air} A_{wall} \quad (46)$$

where $\vec{\tau}_{edge\,i}$ is the viscous shear along the edges of the film cell, $\vec{\tau}_{wall}$ is the wall shear, and $\vec{\tau}_{liq/air}$ is the shear at the liquid-gas interface.

The liquid film Eqs. (40) and (41) can be numerically solved using a predictor-corrector scheme.

4. Impinging Liquid Sheet

The initial thickness of the film formed by an impinging liquid jet on the pre-filmer can be alternatively calculated by other methods instead of using a liquid film model. The liquid jet impinging on an inclined wall was considered by Taylor (1966) and Naber and Reitz (1988). The film sheet thickness for an impinging jet at angular position ϕ was assumed to be given by

$$h_i(\phi)=h_\pi e^{\gamma\left[1-\frac{\phi}{\pi}\right]} \quad (47)$$

where γ is decay parameter.

Figure 8 shows the sheet formed by impinging jets. If the sheet thickness is obtained from the two impinging liquid jets, half thickness can be considered as the impinging thickness on the solid wall or pre-filmer of the gas turbine. The initial sheet thickness (h_i) formed by impinging jets with impinging angle 2(has the following form (Ibrahim and Przekwas, 1991).

$$h_i(\phi)=\frac{(\gamma d_j \sin\theta)\, e^{\gamma\left[1-\frac{\phi}{\pi}\right]}}{2(e^\gamma-1)} \quad (48)$$

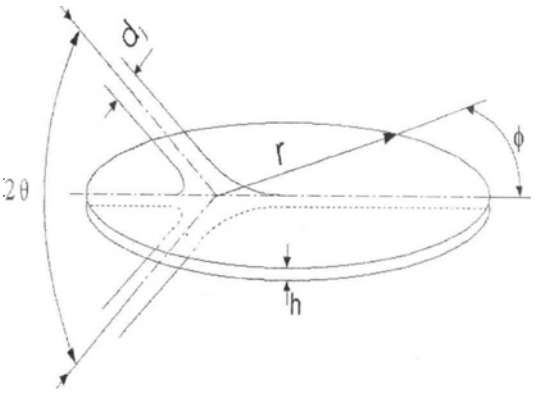

Fig. 8 Sheet formed by impinging jets

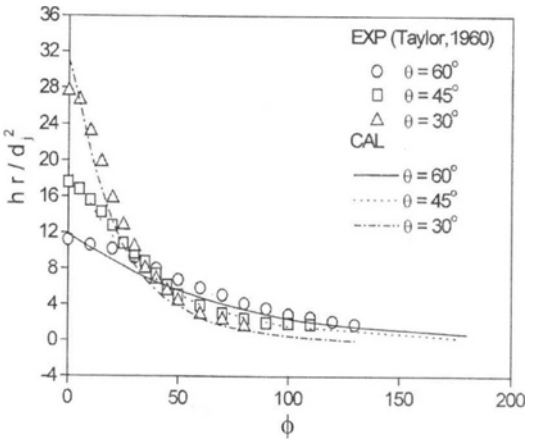

Fig. 9 Variation of liquid sheet thickness

where d_j is the diameter of the jet, θ is the half-impinging angle, ϕ is the angular position coordinate, and γ is the decay factor. The decay parameter, γ, can be determined from the mass and momentum conservation equations, which can be calculated from the following equation using the Newton-Raphson technique

$$\cos\theta=\left(\frac{e^{\gamma+1}}{e^{\gamma-1}}\right)\left[\frac{1}{1+(\pi/\gamma)^2}\right] \quad (49)$$

The thickness of an attenuating sheet, h, is as follows (Ibrahim and Przekwas, 1991);

$$\frac{h}{h_i(\phi)}=\left(\frac{d_j/2}{\sin\theta}\right)\frac{1}{\gamma} \quad (50)$$

where γ is the radial coordinate originating from the impact point. Inspection of Eq. (50) indicates that the sheet thickness is inversely proportional to the distance from the impinging point. Figure

9 shows the variation of dimensionless thickness parameter, $h \cdot \gamma / d_j^2$, predicted by Eq. (50) and obtained by experimental method (Taylor, 1960).

5. Breakup of Liquid Sheet

The liquid sheet formed on the pre-filmer interacts with the swirling air and forms ligaments and droplets. The breakup of the liquid sheet into ligaments and drops is governed by the balance of the forces which are caused by pressure, surface tension, liquid inertia, and viscosity. The time for the disturbance wave to grow to its maximum value at breakup is determined from the resulting equation of motion (Fan and Reitz, 2000).

Dombrowski and Johns (1963) derived a dispersion relation for the growth rate of long waves on the surface of liquid sheet. They identified the wavelength with the largest growth rate and assumed that this wave breaks the sheet into ligaments at half wavelength intervals. The ligaments then break up into drops according to Weber's theory for cylindrical liquid column. Figure 10 shows successive stages in the idealized disintegration of a liquid. Senecal et al. (2000) derived a simplified dispersion relation between growth rate and wavelength for sinuous waves of thin, viscous liquid sheet in a gas. This dispersion relation is used to predict the maximum unstable growth rate and wavelength, the sheet breakup length and the resulting droplet sizes for prefilming airblast injector. The long wave regime is dominant for low-speed sheet atomization, while short waves are responsible for breakup in the case of high speed sheets.

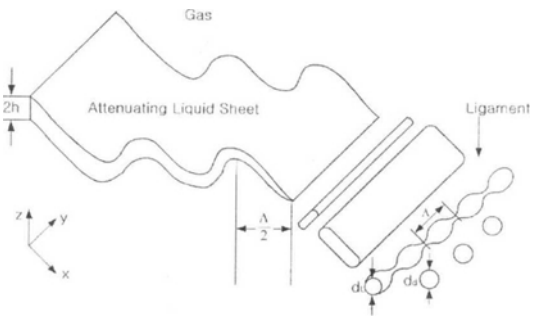

Fig. 10 Successive stages in idealized disintegration of a liquid sheet

5.1 Ligaments in long wave regime and short wave regime

Suppose a liquid sheet of thickness $2h$ is moving with relative velocity U in an inviscid incompressible gas. When low gas Weber numbers, We_2 $\left(=\frac{\rho_2 U^2 h}{\sigma}\right)$, is less than $\frac{27}{16}$, long waves tends to grow on the interfaces and the liquid sheet is broken up by the long waves. The viscous dispersion relation between w and k is

$$\omega_r = -2\nu_1 k^2 + \sqrt{4\nu_1^2 k^4 + \frac{QU^2 k}{h} - \frac{\sigma k^2}{\rho_1 h}} \quad (51)$$

where k is wave number, $Q=\rho_2/\rho_1$, h is the half thickness of the sheet, U is the relative velocity, and w_r is the grow rate. Subsripts 1 and 2 designate liquid and gas, respectively.

In this regime, the effect of viscosity is unimportant. The analysis of inviscid and viscous flow leads to almost the same result as that of inviscid flow for long waves. According to the inviscid analysis, the most unstable wave number is

$$k_s = \frac{\rho_2 U^2}{2\sigma} \quad (52)$$

and the dimensionless maximum growth rate is

$$\left[\frac{\Omega_s h}{U}\right]_{long} = \frac{1}{2}\sqrt{QWe_2} \quad (53)$$

Ligaments are assumed in short wave regime for high-speed sheets (We_2 is greater than 27/16) and $Q \ll 1$. Short waves produce maximum growth rate. Most liquid fuel spray in the propulsion system are high enough that the Weber number is above the critical value. The viscous dispersion relation between w and k is

$$\omega_r = -2\nu_1 k^2 + \sqrt{4\nu_1^2 k^4 + QUk^2 - \frac{\sigma k^3}{\rho_1}} \quad (54)$$

The maximum growth rate (Ω_s) and corresponding wave length ($\Lambda_s = 2\pi/k_s$) can be calculated via Muller's method (Muller, 1956).

5.2 Breakup time

In order to predict the onset of ligament for short wave growth, a sheet breakup length should be calculated. Before reaching the breakup length,

the liquid sheet from the prefilming lip represents an intact sheet, consisting of discrete blob, which has a characteristic size equal to the thickness of the sheet. After reaching the breakup length, the liquid sheet breaks up to ligaments, which are subsequently disintegrated into drops.

At low sheet velocities (i.e., small Weber numbers in the Rayleigh breakup regime), it is reasonable to assume that disruption of the sheet occurs when the amplitude of the dominant wave is equal to the half thickness of the sheet at breakup. The breakup time τ can be evaluated via :

$$\eta_b=\eta_o \exp(\Omega_s \tau) \Rightarrow \frac{1}{\Omega_s}\ln\left(\frac{\eta_b}{\eta_o}\right) \tag{55}$$

where η_o and η_b are the initial wave amplitude and wave amplitude at breakup, respectively.

Thus, the sheet will breakup at the length given by

$$L=V\tau=\frac{V}{\Omega_s}\ln\left(\frac{\eta_b}{\eta_o}\right) \tag{56}$$

where Ω_s is the maximum growth rate obtained from Eqs (51) and (54) as a function of k. The quantity $\ln\left(\frac{\eta_b}{\eta_o}\right)$ has been determined experimentally to be roughly equal to 12. V is the absolute velocity of liquid sheet.

For an attenuation sheet like $h=J/t$, where J is a constant, the thickness is inversely proportional to the radial distance from the injector nozzle. The growth rate must be integrated over time, such that the total growth is used to predict the breakup length for long waves. The expression for the breakup length of the sheet is

$$L=V\left[3\ln\left(\frac{\eta_b}{\eta_o}\right)\right]^{\frac{2}{3}}\left(\frac{J/\sigma}{Q^2U^4\rho_1}\right)^{1/3} \tag{57}$$

5.3 Drop size

In the long wave regime, it is assumed that the ligaments are formed from tears in the sheets twice per wavelength, and the resulting diameter of ligament is given by

$$d_L=\sqrt{\frac{8h}{k_s}} \tag{58}$$

where k_s is the wave number corresponding to the maximum growth rate Ω_s and it is determined from Eq. (52) In the short wave regime, it is assumed that ligaments are formed from tears in the sheet once per wavelength and the resulting wavelength becomes

$$d_L=\sqrt{\frac{16h}{k_s}} \tag{59}$$

where k_s is determined from Eq. (54)

The breakup occurs when the amplitude of the unstable waves is equal to the radius of a ligament, and one drop will be formed per wavelength. A mass balance then gives the drop size,

$$d_d^3=\frac{3\pi d_L^2}{k_L} \tag{60}$$

where k_L is determined from

$$k_L d_L=\left[\frac{1}{2}+\frac{3\mu_1}{2(\rho_1\sigma d_L)^{1/2}}\right]^{1/2} \tag{61}$$

Substitution of Eq. (61) into Eq. (60) gives

$$d_d=1.88d_L(1+3Oh)^{1/6} \tag{62}$$

where $Oh=\mu_1/(\rho_1\sigma d_L)^{1/2}$ is the Ohnesorge number.

The actual drop size is chosen from a specific drop size distribution such as the Rosin-Rammler, log-normal , or Chi-square distribution. At the point of primary breakup of the liquid sheet, droplets are tracked using the Lagrangian approach, a parcel of physically similar drops (i.e. similar kinetic and thermodynamic properties) can be used to simplify the numerical treatment.

Recently Zuo et al. (2002) applied this liquid sheet break model to the spray in the cross flow for the gas turbine combustor. Zuo et al. (2002) compared the spray structure of the liquid jets atomized in subsonic crossflows with the experimental data of Wu et al. (1997). Simulated spray distribution agrees well with the experimental shadowgraph. Zuo et al. (2002) did not modeled the wake flow behind the liquid jet column and then his application of sheet breakup model to cross flow is quite reasonably agreeable with the experiments except behind liquid column.

The large droplets formed from a liquid sheet may disintegrate into smaller droplets when instability conditions are satisfied. Two types of secondary droplet breakup can be considered as explained in section 2. The one is wave models

which are based on the instability of wave. The other is TAB (Taylor Analogy Breakup) model which is based on Taylor's analogy between an oscillating and distorting drop and a spring-mass system. At high speed air stream wave model is better than TAB model as shown in section 2.

Summary

The performance of swirl type of atomizer in gas turbine is affected mostly by the shear stress between the air jets that swirl in opposite directions. A dome swirler is additionally used to provide good spray patternation and adequate droplet dispersion in the combustor. The spray formed by high-shear nozzle/swirler assembly has several characteristics such as liquid column injection, wall impingement, wall film, liquid sheet breakup, and secondary droplet breakup. Part of the spray models were validated with experimental data.

For the initial calculation of liquid jet from a hole type nozzle in high-shear nozzle assembly of the gas turbine, liquid blob breakup can be modeled using Kelvin-Helmholtz, Rayleigh-taylor instability, or hybrid liquid breakup model. Hybrid model showed good agreement with the experimental data obtained by PDPA. On the wall of the pre-filmer of the combustor, droplet-wall interaction model and liquid film model can be applied. A linear stability analysis is introduced for high-speed viscous liquid sheet atomization on the pre-filmer of the gas turbine. A larger droplet from a liquid sheet may disintegrate into smaller droplet and this can be modeled using a wave model or TAB model. At high air stream, wave model is better than TAB model, but at low speed air stream wave model or TAB model both can be applied. The liquid sheet breakup model could be successfully applied to the spray in crossflow which is found in the gas turbine engine.

References

Aigner, M. and Wittig, S., 1987, "Swirl and Counter Swirl Effects in Prefilming Airblast Atomizers," ASME Paper 87-GT-204.

Amsden, A. A., O'rourke, P. J. and Butler, T. D., 1989, "KIVA-II - A Computer Program for Chemically Reactive Flows with Sprays," Los Alamos National Labs., LA-11560-MS.

Bai, C. and Gosman, A. D., 1996, "Mathmatical Modeling of Wall Films Formed by Impinging Sprays," SAE Paper 960626.

Bower, G. R., Chang, S. K., Corradini, M. L., El-Beshbeeshy, M., Martin, J. K. and Krueger, J., 1988, "Physical Mechanisms for Atomization of a Jet Spray : A Comparison of Models and Experiments," SAE Trans., Vol. 97, SAE Paper No. 881318.

Chang, S. K., Koo, J. Y. and Chung, H. C., 1995, "Transient Liquid Jet Breakup Model and Comparison with Phase Doppler Measurements," KSME International Journal Vol. 9, No. 1, pp. 41~50.

Cohen, J. M. and Rosfjord, T. J., 1993, "Influences on the Sprays Formed by High-Shear Fuel Nozzle/Swirler Assemblies," Journal of Propulsion and Power, Vol. 9, No. 1, pp. 16~27.

Dombrowski, N. and Johns, W. R., 1963, "The Aerodynamic Instability and Disintegration of Viscous Liquid Sheets," Chemical Engineering Science, Vol. 18, pp. 203~214.

Fan, L. and Reitz, R. D., 2000, "Spray and Combustion Modeling in Gasoline Direct-Injection Engines," Atomization and Sprays, Vol. 10, pp. 219~249.

Foucart, H., Habchi, J. F., Le Coz, J. F. and Baritaud, 1988, "Development of a Three Dimensional Model of Wall Fuel Liquid Film for Internal Combustion Engines," SAE Paper 980133.

Hiroyasu, H. and Arai, M., 1990, "Structures of Fuel Sprays in Diesel Engines," SAE paper 900475.

Hwang, S. S. and Koo, J. Y., 1997, "Modeling the Atomization of Fuel Droplets in High Speed Air Stream," Proceedings of the 30th International Symposium on automotive & Automation, pp. 279~284.

Ibrahim, E. A. and Przekwas, A. J., 1991, "Impinging Jets Atomization," Phys. Fluids A 3 (12), pp. 2981-2987.

Lin, S. P. and Reitz, R. D., 1988, "Drop and

Spray Formation from a Liquid Jet," Annu. Rev. Fluid Mech. Vol. 30, pp. 85~105.

Mansour, A., Benjamine, M. A. and Steinthorsson, E., 2000, "A New Hybrid Air Blast Nozzle for Advanced Gas Turbine Combustor," ASME Paper 2000-GT-117.

Matsumoto, S. and Saito, S., 1970, "On the Mechanism of Suspension of Particles in Horizontal Conveying : Monte Carlo Simulation Based on the Irregular Bouncing Model," (Japanese) J. Chem. Engr., Vol. 3, pp. 83~92.

Muller, D. E., 1956, "A Method for Solving Algebraic Equations Using an Automatic Computer," Mathematics of Computation, Vol. 10, pp. 208~215.

Naber, J. D. and Reitz, R. D., 1988, "Modeling Engine Spray/Wall Impingement," SAE Paper 880107.

O'Rourke P. J. and Amsden, A. A., 1987, "The Tab Method for Numerical Calculation of Spray Droplet Breakup," SAE Paper 872089.

Nicholls, J., 1972, "Stream and Droplet Breakup by Shock Waves," NASA SP-194, pp. 126~128.

Pilch, M., 1981, "Acceleration Induced Fragmentation of Liquid Drops," University of Virginia, Ph. D. Thesis.

Pilch, M. and Erdman, C. A., 1987, "Use of Breakup Time Data and Velocity History Data to Predict the Maximum Size of Stable Fragments for Acceleration-Induced Breakup of a Liquid Drop," Int. J. Multiphase Flow, Vol. 13, No. 6, pp. 741~757.

Ranger, A. A. and Nicholls, J. A., 1969, "Aerodynamic Shattering of Liquid Drops," AIAA Journal Vol. 7, No. 2, pp. 285~289.

Reitz, R. D. and Bracco, F. V., 1979, "On the Dependence of Spray Angle and Other Spray Parameters on the Nozzle Design and operating Conditions," SAE Paper 790494.

Reitz, R. D. and Diwakar, R., 1986, "Effects of Drop Breakup on Fuel Sparys," SAE paper 860469.

Reitz, R. D., 1987, "Modeling Atomization Processes in High-Pressure Vaporizing Sprays," Atomisation and Spray Technology, Vol. 3, pp. 309~337.

Reitz, R. D., 1994, "Computer Modeling of Sprays," Spray Technology Short Course Note, Pittsburgh, PA, May 17.

Rosskamp, H., Willmann, M., Meisl, J., Meier, R., Maier, G. and Wittig, S., 1998, "Effect of the Shear Driven Liquid Wall Film on the Performance of Prefimming Airblast Atomizer," ASME Paper 98-GT-500.

Senecal, P. K., Schmidt, D. P., Nouar, I., Rutland, C. J., Reitz, R. D. and Corradini, M. L., 1999, "Modeling High- Speed Viscous Liquid Sheet Atomization," International Journal of Multiphase Flows 25, pp. 1073-1097.

Simpkins, P. G. and Bales, E. L., 1972, "Water-Drop Response to Sudden Accelerations," J. Fluid Mech., Vol. 55, Part 4, pp. 629~639.

Stanton, D. W. and Rutland C. J., 1996, "Modeling of Film Formation and Wall Interaction in Diesel Engines," SAE Paper 960628.

Stanton, D. W. and Rutland C. J., 1998, "Multi-Dimensional Modeling of Heat and Mass Transfer of Fuel Films Resulting from Impinging Sprays," SAE Paper 980132.

Taylor, G. I., 1960, "Formation of Thin Flat Sheets of Water," Proceedings of Royal Society, London, Vol. 259A, pp. 1~17.

Taylor, G. I., 1963, "The Instability of Liquid Surfaces When Accelerated in a Direction Perpendicular to Their Planes. I," The Scientific Papers of G. I. Taylor Vol. 3, pp. 532~536, edited by Batchelor, G. K., Cambridge University Press

Taylor, G. I., 1966, "Oblique Impact of a Jet on a Plane Surface," Phil. Trans. Roy. Soc. (London) A, Vol. 260, pp. 96~100.

Wu, P. K., Kirkendall, K. A., Fuller, R. P. and Nejad, A. S., 1997, "Breakup Processes of Liquid Jets in Subsonic Crossflows," Journal of Propulsion and Power, Vol. 13, No. 1, pp. 64~73.

Zuo, B., Black, D. L. and Crocker, D. S., 2002, "Fuel Atomization and Drop Breakup Models for Advanced Combustion CFD Codes," AIAA Paper 2002-4175.

Xin, J., Ricart, L. and Reitz, R. D., 1998, "Computer Modeling of Diesel Spray Atomization and Combustion," Combust. Sci. and Tech., Vol. 137, pp. 171~194.